Research Article

Zhi-He Xu, Zhen-Jun Sun*, Wei Xin, and Liping Zhong

Geothermal resource potential assessment of Erdaobaihe, Changbaishan volcanic field: Constraints from geophysics

https://doi.org/10.1515/geo-2020-0282
received March 22, 2021; accepted July 20, 2021

Abstract: Geothermal resources occurring in the Changbaishan volcanic field are directly or indirectly controlled by volcanic activity and exhibit a close correlation with deep-seated faults. Energy and thermal transfer are generally controlled by groundwater circulation and hot gas emission. This article considers the detectability of hot water and gas by geophysical methods. The controlled source acoustic magnetotelluric (CSAMT) and radon (^{222}Rn) gas methods give straightforward information on electrical resistivity and natural radon emissions, respectively, to assess the geothermal condition. The CSAMT method detected five-banded low-apparent resistivity bodies (decreasing from 3,000 to 300 Ωm), indicating that there exists a high degree of water-bearing capacities in the subsurface. The radon (^{222}Rn) gas concentrations were monitored in two rapid growth zones: one zone showing values ranging from 3,000 to 23,000 Bq/m^3, and the other with values from 4,000 to 24,000 Bq/m^3. These changes demonstrate that the heat energies available in these areas were very high and that there is potential for geothermal resources in those zones. Combining with previously published data from geothermometry and geothermal drilling, we argue that there is great potential in Erdaobaihe for geothermal exploitation and that the geothermal resource type should be classified into uplift mountain geothermal system no magma type.

Keywords: geothermal resource, Changbaishan volcanic field, controlled source acoustic magnetotelluric, radon gas

1 Introduction

Geothermal resources, as an alternative source of energy, are generally developed in areas where volcanism and magmatism have been active since the Late Cenozoic (i.e., the Jingbohu, Wudalianchi, and Tengchong geothermal fields) [1,2]. As one of three active volcanoes in China, the Changbaishan volcanic field saw eruptions in 1668, 1702, and 1903 AD, which were high-intensity explosive eruptions and demonstrated favorable geothermal resource potential [3]. The location of each hot spot in the Changbaishan geothermal field (CHGF) exhibits a close correlation with the fault that transfers the geothermal flow from the deep magma chamber to shallower depths [4,5]. Therefore, assessing the geothermal resource potential of the periphery of the CHGF is of great possible value.

However, the majority of efforts in this area to exploit geothermal resources are around the Changbaishan volcano (e.g., Lake Shoreline, Julong, and Jinjiang geothermal fields). There is not even a hot spring with high economic value and exploitation potential further away from the Changbaishan volcano, which is inconsistent with the classical volcano-geothermal model [3]. This is due to the periphery of Tianchi caldera lacking geophysical data covering the deep faults. In contrast to geothermal drilling, geophysical methods not only acquire in situ information but also allows for the investigation of the outer ring of the geothermal active zones [6]. Controlling factors in the geothermal zone around active volcanoes are mainly associated with faults, magma chambers, and the distribution of subsurface water. The application of multiparametric geophysical methods can provide adequate information to delineate the complicated geological bodies at different

* **Corresponding author: Zhen-Jun Sun,** Institute of Disaster Prevention, Sanhe City, 065201, People's Republic of China; Hebei Key Laboratory of Earthquake Dynamics, Sanhe City, 065201, People's Republic of China, e-mail: 110357960@qq.com
Zhi-He Xu: Institute of Disaster Prevention, Sanhe City, 065201, People's Republic of China; Hebei Key Laboratory of Earthquake Dynamics, Sanhe City, 065201, People's Republic of China
Wei Xin: College of Earth Science and Engineering, Shandong University of Science and Technology, Qingdao 266590, People's Republic of China
Liping Zhong: Jilin Exploration Geophysics Institute, Changchun City, 130012, People's Republic of China

depths. Moreover, Erdaobaihe located at the foot of the Changbaishan, 25 km north of the Tianchi caldera, enjoys favorable advantages in terms of location and geological conditions. Therefore, in this work we present results from surveys undertaken using the advanced controlled source audio-frequency magnetotellurics (CSAMT) method, which displays great depth penetration, to uncover the migration pathways of hot water and the radon (^{222}Rn) gas method to assess the heat energy and to confirm the inferences made from the analysis of the CSAMT data.

2 Geological setting

2.1 Regional setting

The CHGF is located between the inland of the Eurasian Plate and the Pacific subduction zone [7]. There are three polygenetic volcanoes dominated by basaltic to silicic volcanic rock suites: Tianchi, Wangtian'e, and Namphothe. More than 200 monogenetic volcanoes that erupt basaltic products are sporadically scattered around these polygenetic volcanoes [8]. During the Late Mesozoic to Cenozoic, the tectonic evolution of the CHGF was dominated by the subduction of the Pacific plate with the products of volcanic activity (e.g., volcanic cones, basalts lava plateau, ash, pumice, and pyroclastic flows) being prominent in the Eurasian plate, particularly in the CHGF [9,10] (Figure 1). The regional fractures of the CHGF are dominated by northeast (NE), north-west (NW), and north-south (NS) trending faults [11]. These faults can be categorized into two types: (1) the NW and NE older faults, which are suggested to be related to the successive subduction of the Pacific plates in the eastern margin of the Eurasian continent; and (2) the NS young faults, which are associated with Late Cenozoic volcanic activity and form the Julong hot spring.

Medium-temperature geothermal resources are generally clustered around the Tianchi caldera or in the valleys around the cone, such as the Hubin, Julong, and Jinjiang hot springs. Low-temperature geothermal resources are scattered further away from the Tianchi caldera, such as Erdaobaihe and Songjianghe [14]. The formation of these hot springs is a consequence of the continuous advection of heat and groundwater from the activation of the Changbaishan volcano [15] (Figure 2).

2.2 Local setting

The Cenozoic Manjiang formation is widely distributed around Erdaobaihe and the Junjianshan formation is locally exposed on the western side. The former's lithology is amygdaloidal basalt and the latter's is massive black basalt. The Mesoproterozoic Daxing formation occurs sporadically in the center of the GHGF and is mainly composed of quartz

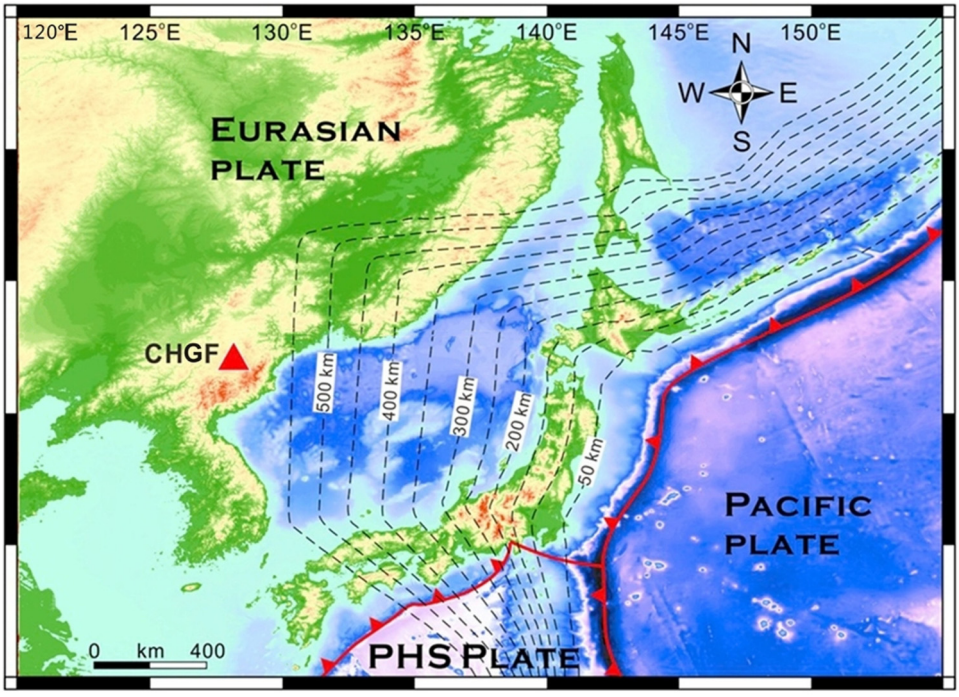

Figure 1: Simplified map showing the location of the CHGF within the context of the continental intraplate framework. The red lines show the movement direction of the Pacific and Philippine Sea (PHS) plates. The black dotted lines represent the present boundary of the subducting of the Pacific slab [12].

sandstone, sericite quartz sandstone, chlorite, and epidote. The Mesoproterozoic Wangdeshan formation is exposed in the northern and southern sides, and the strata are composed of dolomitic marble, altered marble, and brecciated marble. The Late Permian intrusion occurs sporadically around the eastern side and the lithology is medium fine-grained monzogranite. Due to the sporadic exposure and widespread Quaternary basalts, the extent of the Tianchi-Erdaobaihe fault is difficult to identify. Three ascending springs were discovered in the middle of the geophysical profile (Figure 3).

3 Geophysical analytical techniques

3.1 Controlled source audio-frequency magnetotellurics

CSAMT data were collected along a west–east-trending section (5 km), which cuts across the south–north-trending faults. This section included 251 CSAMT sites at intervals of 20 m. It was surveyed with the multifunctional electric exploration system V8 (Phoenix Corporation, Canada). The V8 receivers, a 16-bit high-frequency signal, and 24-bit low-frequency signal instrument have a high dynamic range and resolution. The horizontal electric dipole transmitter was located at E 128°8′18″, N 42°23′14″, and the emission current was about 20 A. The distance between the transmitter and receiver was 9.5 km. The scalar mode was used for the measurements, and the frequency band was set from 1 to 9,600 Hz (Figure 4). We used a high-frequency AMTC-30 sensor and solid nonpolarized poles for collecting magnetic and electric field signals, respectively.

Before inversion, the raw data were evaluated and preliminary data processing was carried out to ensure the data quality. First, we used a 50 Hz notch filter to remove the industrial noise. Figure 5 displays the Cagniard resistivity and impedance phase of each CSAMT site. The curves in the pseudosection map are smooth, which indicates that the raw data are reliable. Then, a low-pass Hanning window spatial filter was applied to eliminate the static effect. Finally, the resistivity

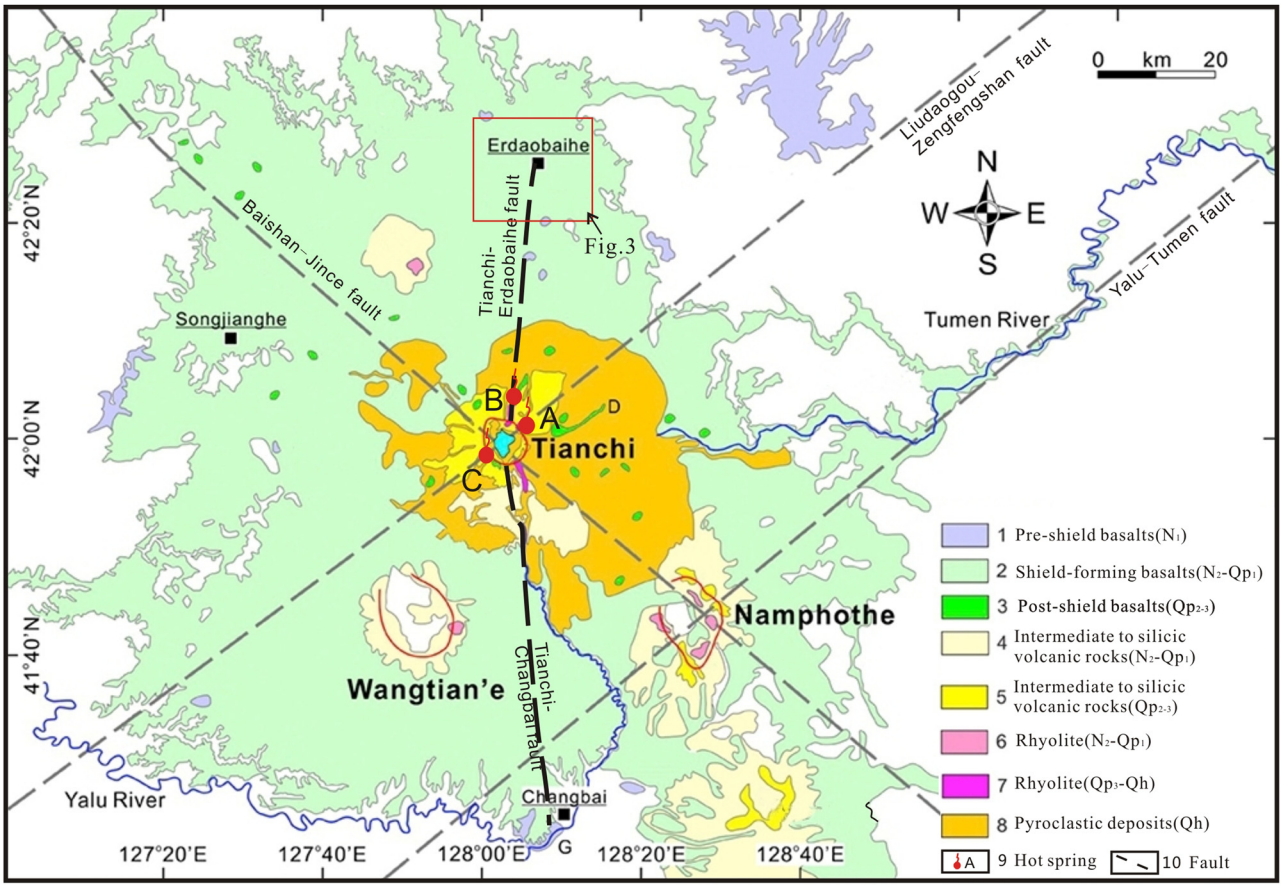

Figure 2: Simplified regional geological map of the CHGF (modified from Qian et al., 2014 [13]), showing the locations of hot springs. Typical localities of hot springs are labeled as follows: (A) Hubin, (B) Julong, and (C) Jinjiang.

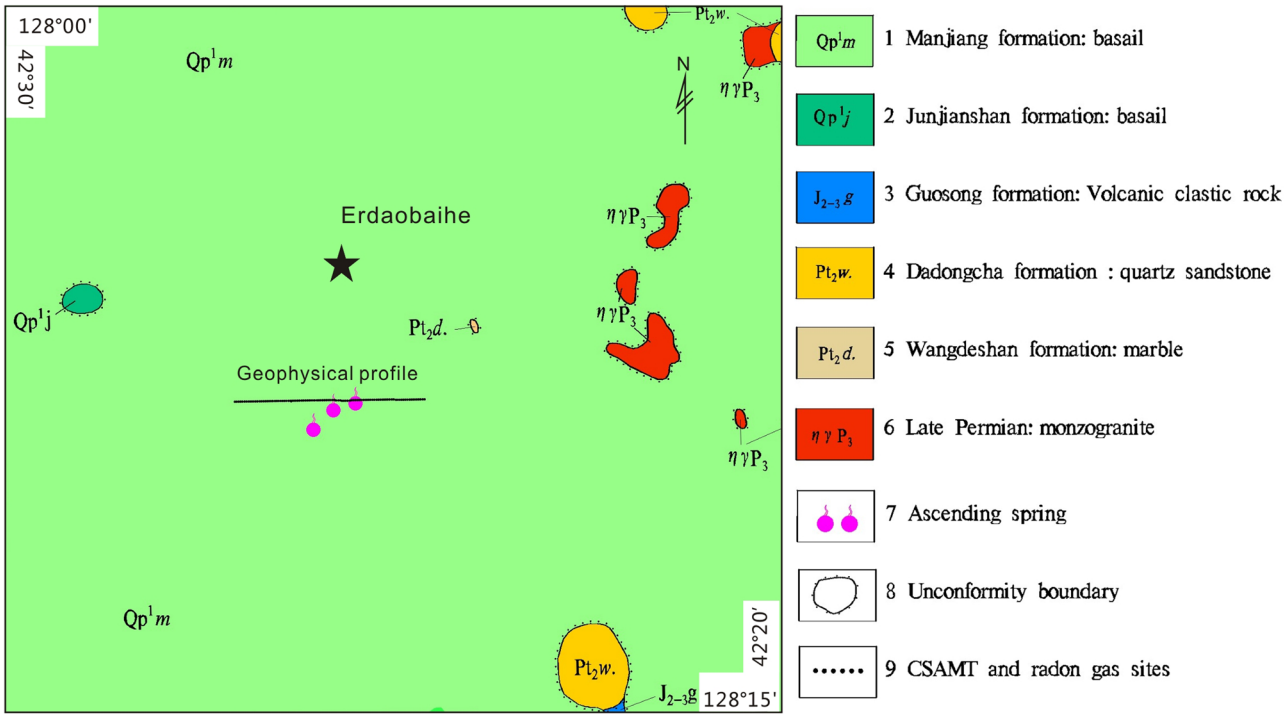

Figure 3: Simplified geological map of Erdaobaihe, showing the locations of CSAMT and radon gas samplings (unpublished).

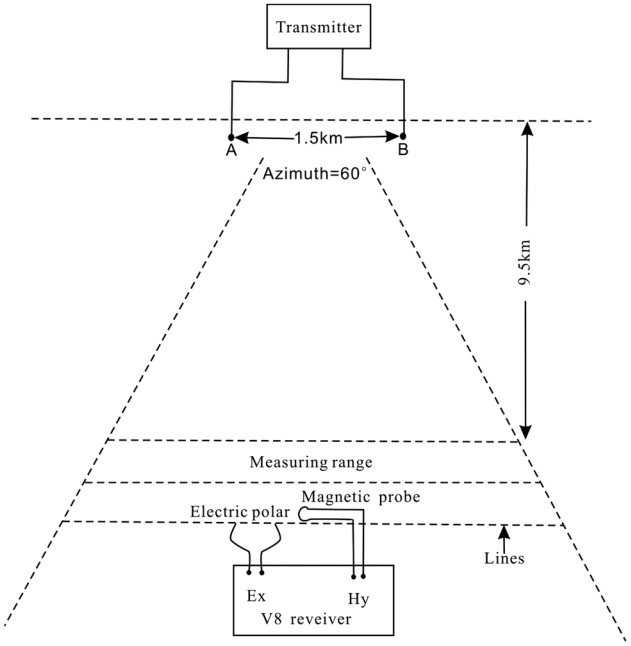

Figure 4: An outline of the CSAMT field survey undertaken for this work. The transmitter provides the electromagnetic signal at different frequencies, and the receivers measured the electrical and magnetic signals in the far-field with the polar and magnetic probe, respectively. A and B represent the transmitter electrodes.

inversion was carried out using the commercial software Scs2D.exe (Zonge Company, United States of America). The adoption of transverse electric (TE) and transverse magnetic (TM) modes for the inversion is more in accord with the geological model. After three iterations, the overall root mean square misfit was reduced to 1.13.

3.2 Radon gas survey

A total of 251 samples were measured using an FD-3017 type radon gas detector (Shanghaishenke Corporation, China) [16]. The measurement accuracy of this type of active detector is 0.1 Bq/m^3, with a sample spacing of 20 m along the same profile as the CSAMT survey. The measurement duration was 2 min. The workflow of the FD-3017 equipment is as follows. First, a pilot hole is drilled by the fine steel in the soil, and the radon gas sampler is inserted into the drilled hole to a depth of more than 0.7 m. Then, the air pump is lifted to the high position, and the valve is closed to isolate the gas in the cylinder desiccant from the outside. The field radon gas is then captured in the reactor. Finally, high pressure is applied for measuring the radon gas underground in the air pump (Figure 6).

The water chemistry iteration method was adopted for radon gas data processing. First, we calculate the average value (X_1) and the standard deviation (SD_1). Then, a new data set is obtained by eliminating those

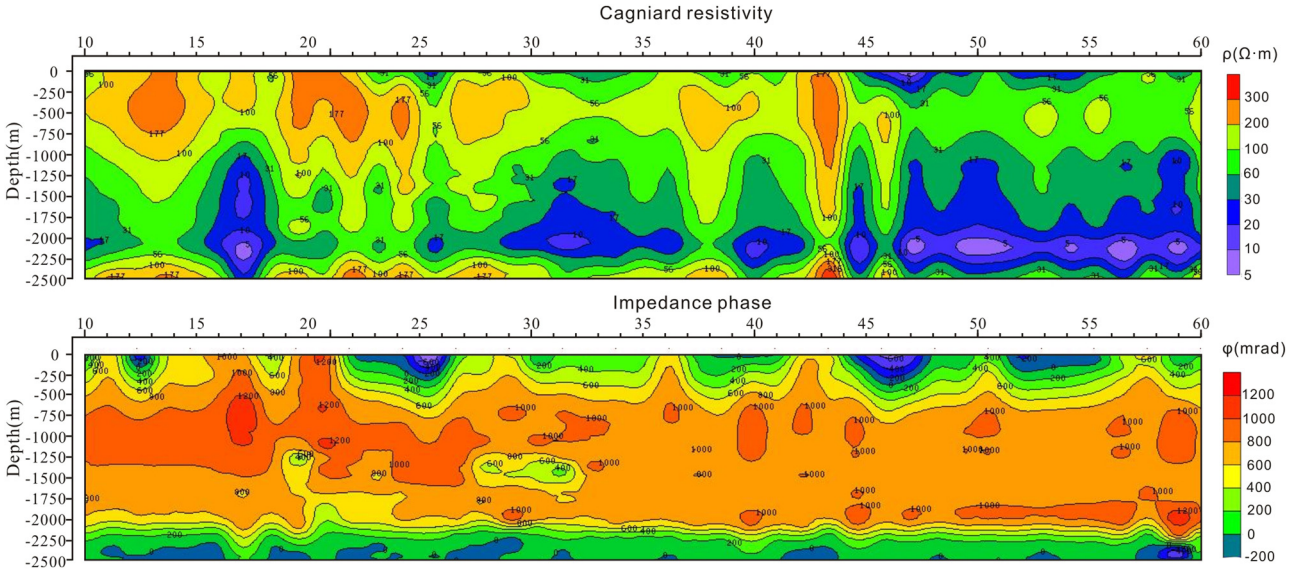

Figure 5: The pseudosection of the Cagniard resistivity and impedance phase map derived from the CSAMT profile. The *X*-axis shows the site locations and the *Y*-axis shows the frequency of each site.

higher values that were more than three times the standard deviation from the average. The previous steps are then repeated until no higher values appear. Eventually, the final average is calculated, and the background value is set as 3,000 Bq/m^3. Moreover, according to the formulas $X_1 + 0.5SD_1$, $X_1 + 2SD_1$, and $X_1 + 3SD_1$, the radon data are divided into a normal zone, a medium anomalous zone, and a high anomalous zone, respectively.

4 Results

4.1 CSAMT results

The CSAMT results provided a high resolved resistivity section of the crust in Erdaobaihe (Figure 7b). From the surface to an elevation of around 600 m, the CSAMT profile shows high resistivity, which is associated with

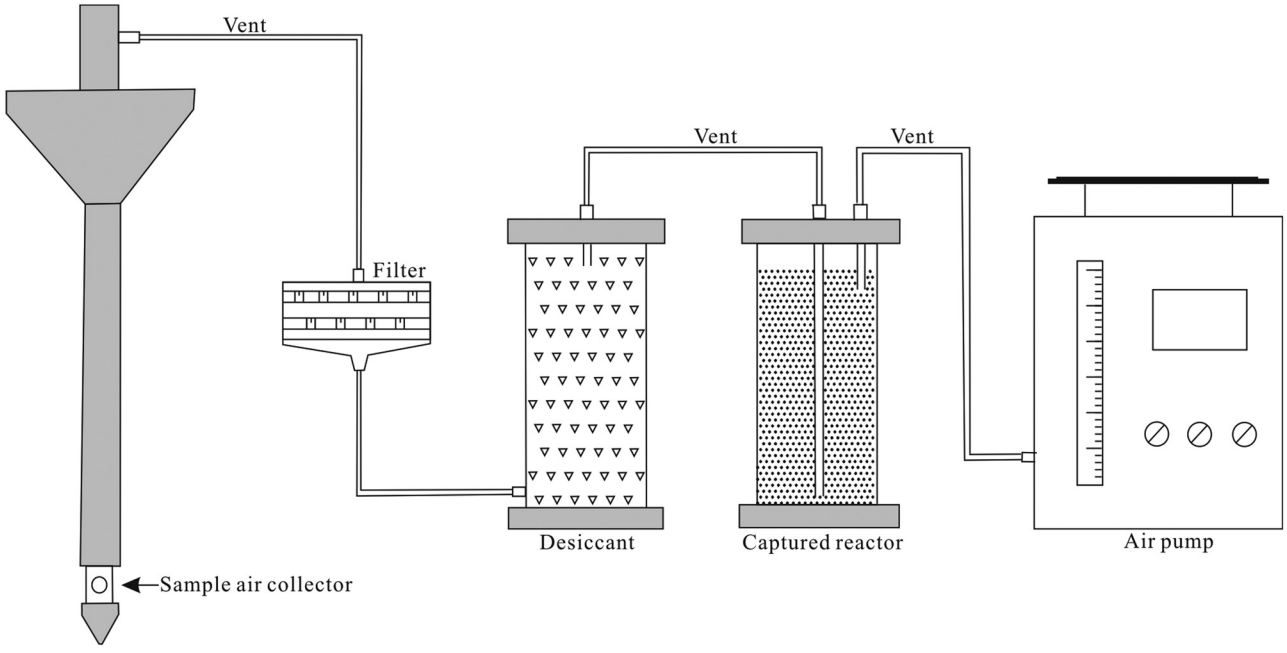

Figure 6: Schematic diagram of the sampling process using the active radon (^{222}Rn) gas detector.

basalts. From 600 to 0 m, between sites 10 and 23, the intermediate apparent resistivity is associated with the volcanoclastic rock and quartzose sandstone (Figure 7b). Based on the regional physical properties and drilling data [17], we suggest that the deeper subsurface geological body (high resistivity) consists of marble with undeveloped fractures. At site 23, a sudden physical property change in apparent resistivity (from 3,000 to 300 Ωm) is interpreted as a brittle fracture zone (named F2), which separates quartzose sandstone from marble on the surface. At sites 23–60, the pseudo section of resistivity consists of a widespread high-resistivity anomaly intercalating with some banded low-resistivity anomalies. Regarding the high-resistivity anomaly, this corresponds to the marble which is the typical lithology of the metamorphic basement in Changbaishan. For the low-resistivity anomalies (sites 44, 46, and 48), considering their high water-bearing capacity and strong electrical conductivity, they should be regarded as marble with developed fractures. Moreover, the locations of these

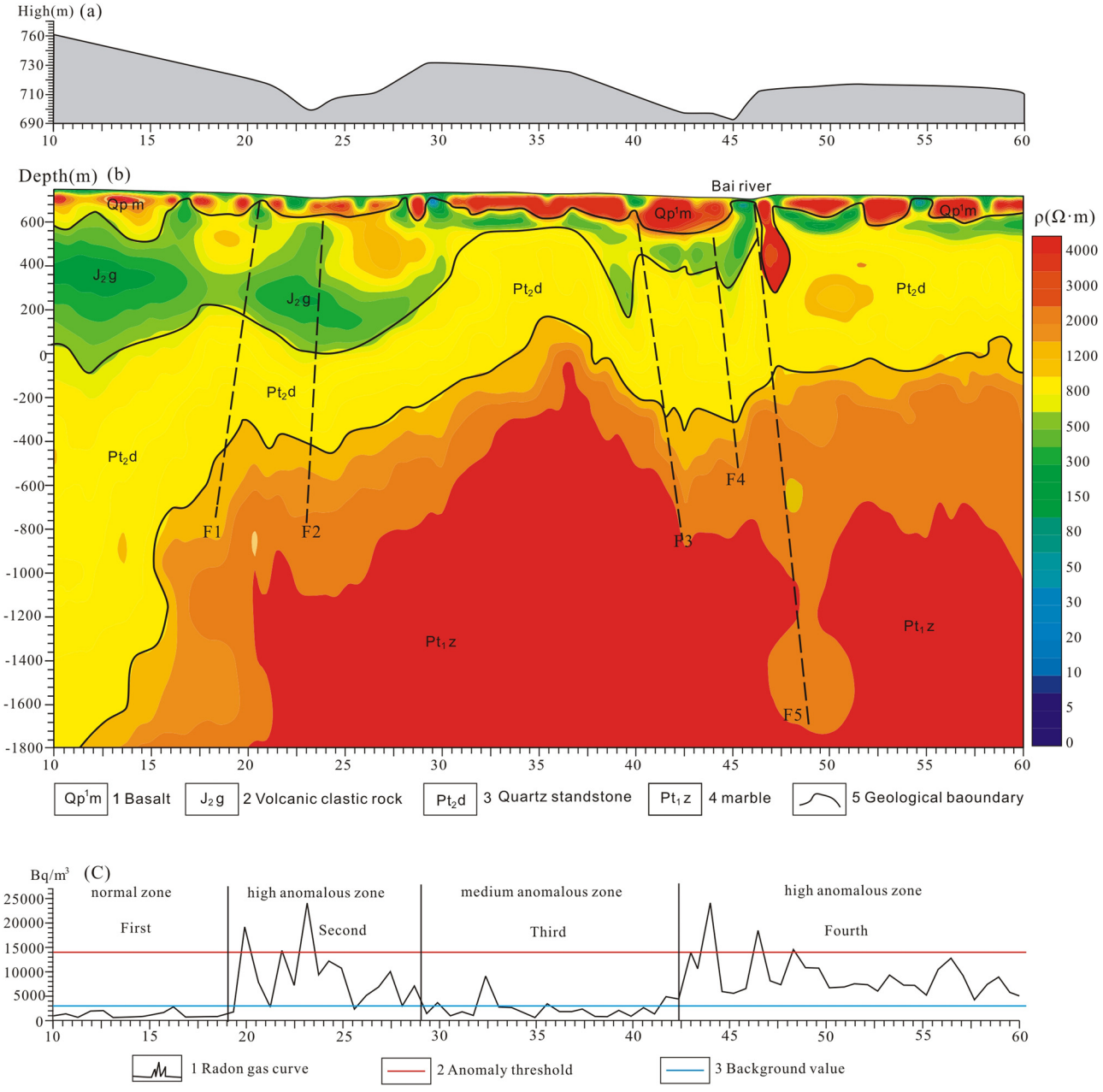

Figure 7: (a) The topographic curve map. (b) The CSAMT nonlinear conjugate gradient inversion map. (c) The cumulative production at each site of radon (^{222}Rn) gas. The *X*-axis shows the site locations.

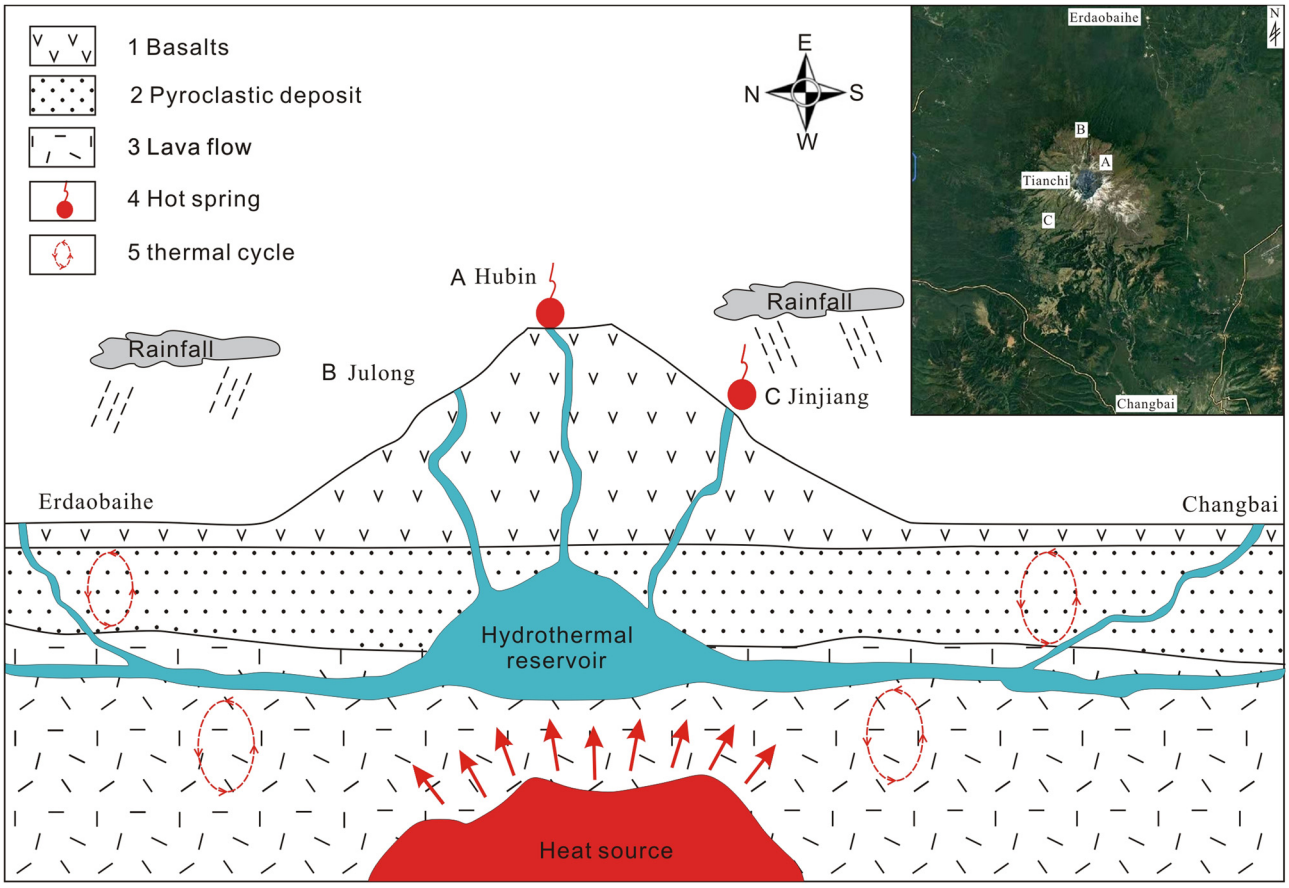

Figure 8: Geological sketch showing the formation of geothermal resources in the CHGF. The inset shows an image of the study area with the Hubin, Julong, and Jinjiang hot springs marked.

low-resistivity anomalies coincided with the low values of the topographic curve (Figure 7a). Combining with the fact that there are three ascending springs near site 44 (Figure 3), we argued that these low-resistivity anomalies above could therefore act as vessels for hot water to migrate from the deep thermal reservoir into shallower crust.

4.2 Radon gas result

The distribution of radon gas is influenced by two factors: water temperature and fracturing. The first factor affects the volatility of radon in hot springs and the second influences the radon gas discharge [16]. Figure 7c presents the cumulative production at each site of radon (^{222}Rn) gas. Based on the curve shape of the radon, part statistics are carried out to eliminate disturbing factors of the radon. Along the profile, the radon distribution was divided into four zones. The first and the third zones have generally low values of radon, indicating low total heat energy or undeveloped fractures. The second and the fourth zones show generally high values, indicating the available heat energy is much greater, suggesting the potential for geothermal exploitation. Moreover, the values in these zones are all significantly higher than the background level (blue horizontal line, Figure 7c). Considering the maximum and minimum values of the measured radon gas, the natural background value and the anomaly threshold should be set to 3,000 and 14,000 Bq/m^3, respectively. Thus, two coniform tooth-shape anomalies are identified at sites 20 and 23 with radon gas values of 19,000 and 24,000 Bq/m^3, respectively. Three bullet tooth-shape anomalies are identified at sites 44, 46, and 48 with values of 24,000, 18,000, and 14,500 Bq/m^3, respectively. These results further verify the locations of fractures presented in Section 4.1.

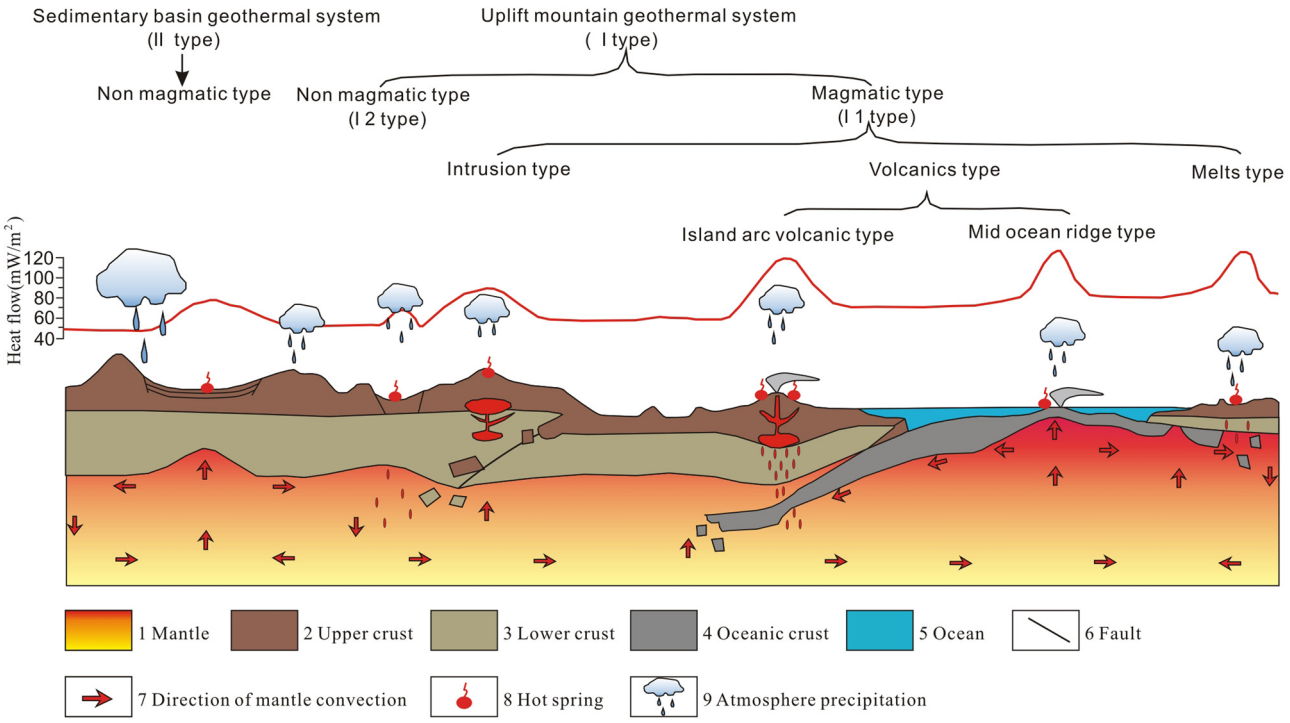

Figure 9: Diagrammatic sketch of a simplified geological cross section of the different types of geothermal systems (modified from Zhang et al. [24]).

5 Discussion

5.1 Geothermal resource potential assessment of Erdaobaihe

As a world-famous active volcanic field, there are many hot springs rising to the shallow surface in the CHGF. This fact indicates that favorable geothermal resource elements for this area are as follows: an abundant heat source, good storage performance, and high levels of fluid migration. However, due to the thick covering of Quaternary basalts in Erdaobaihe, only limited information can be obtained, which makes it difficult for geologists to assess the geothermal potential in this area.

The results from the CSAMT method indicate that the deep geological body is a marble. Abundant low- to medium-temperature hot springs in Italy have shown that marble can act as a reservoir for geothermal resources [18]. High apparent resistivity extending from shallow to greater depths suggests a thick reservoir. Five-banded low-apparent resistivity anomalies indicate that there exist water-bearing fracture zones or karst caves in the marble. Owing to its high storage and drainage capacity, marble is a good reservoir for geothermal resources, especially cracked marble. Combining these results with the regional geological map (Figure 2), these faults are the secondary faults of the Tianchi-Erdaobaihe fault. Widespread faults play an important role in geothermal water movements, such as recharge and discharge. Moreover, these faults are all located in the high-value radon gas zones, which indicate high heat energies and potential geothermal reservoirs. According to previously published data in geothermometry, Erdaobaihe is located in a relatively high-temperature belt in the geothermal anomaly distribution map, with the geothermal gradient greater than 3.0°C/100 m [19]. The deep-seated magma chamber beneath Tianchi directly serves as a heat source for the Hubin, Julong, and Jinjiang hot springs, and then by means of convention it indirectly disseminates heat towards Changbai and Erdaobaihe (Figure 8). Thus, Erdaobaihe has met the aforementioned geothermal resource conditions.

5.2 Geothermal resource in Erdaobaihe

Generally, the classical genesis model of geothermal systems can be classified into two types: the uplift mountain geothermal systems (I type) and sedimentary basin geothermal systems (II type) [20]. According to the basic characteristics of geothermal systems, as described in

Table 1: Basic characteristics of the geothermal system

Classification	**Uplift mountain (I type)**			
Geological setting	Plate margin and interplate uplift			
Subtype	Magmatic type (I1 type)		Nonmagmatic type (I2 type)	
Hot source	Intrusion, volcano, and melts		Radioactive decay, heat conduction	
Heat flow (mW/m^2)	>85		60–100	
Geothermal resource	Hydrothermal type (I1-1 type)	Dry-hot type (I1-2 type)	Hydrothermal type (I2-1 type)	Dry-hot type (I2-2 type)
Water source	Mainly of atmospheric precipitation with minor magmatic water and seawater	Non or only minor magmatic or sedimentary water	Mainly of atmospheric precipitation with minor seawater	Non or only minor sedimentary water
Lithology	Volcanics, intrusion, metamorphic, and sedimentary rocks	Intrusion, metamorphic, and sedimentary rocks	Primarily granite; secondly volcanic, metamorphic, and sedimentary rock	Primarily granite secondly volcanic, metamorphic, and sedimentary rock
Porosity	Mainly of fracture with minor pores	Non or only with minor fracture and pores	Mainly of fracture with minor pores	Non or only with minor fracture and pores
Temperature	>150°C	150–300°C	40–150°C	>150°C
Geothermal distribution	Localization	Universality	Localization	Universality
Geothermal gradient (°C/hm)	>4	>4	>3	>3
Geothermal channel	Fracture development	Locally fracture development	Fracture development	Locally fracture development
Thermal transfer	Convection	Conduction	Convection	Conduction
Classic example	Yambajam, Tibet	Kraft, Iceland	In this paper	Zhangzhou, Fujian

Figure 9, Type I can be further divided into additional subtypes, magmatic (Type I-1) and nonmagmatic (Type I-2) [20]. Information on the geological setting, heat source, heat flow, water resources, lithology, porosity, fluid distribution, and thermal transfer mode is listed in Table 1 and presented in Figure 9 [21]. Based on the results of the CSAMT profiles, no trace of Cenozoic magma has been found underlying Erdaobaihe, while the lithology of the geothermal reservoir is carbonate rocks (marble). Moreover, according to the four deep seismic profiles from Tianchi to Erdaobaihe, there are two magma chambers beneath the Tianchi volcano and the Western Tianchi Protection Station, which further verifies the interpretation inferred from the CSAMT profile [22]. Five-banded low-resistance anomalies (the values <500 Ωm) extending from the subsurface to depths of 800 m below sea level were interpreted to be the fractures developing in the marble. Combined with the results of the radon gas profile, the locations of the fractures discussed above were further confirmed and the geothermal gradient in these sites should be higher than others. The annual precipitation of 1347.3 mm indicates that the water source is atmospheric precipitation [23]. The north-south trending fault could also form steaming grounds and fumaroles during the fluids' ascent to the surface (Figure 2). In addition, considering the distribution of Hubin, Julong, Jinjiang, Changbai, and Erdaobaihe hot springs, the first three should be assigned to the I1-1 type and the latter two are of I2-1 type (Table 1).

6 Conclusions

(1) Based on the results of the CSAMT profile, five-banded low-resistance anomalies regarded as geothermal channels were identified.
(2) The radon gas results further confirmed these fracture locations and the geothermal gradient in these sites should be higher than others.
(3) Erdaobaihe has met the aforementioned conditions for the existence of geothermal resources that could be exploited.
(4) According to the basic characteristics of a geothermal system, Erdaobaihe geothermal resource should be assigned to the I2-1 type.

Acknowledgments: We thank the managing editor, Jan Barabach, for his efforts and patients in dealing with our manuscript. We thank the reviewers' scientific attitude and responsible spirit, from which we have gained a great deal of new knowledge and skills. We gratefully acknowledge the support from the Jilin Provincial Geological Exploration Fund Project [grant number 2018-14].

Funding information: Jilin Provincial Geological Exploration Fund Project [grant number 2018-14].

Author contributions: Z.J.S. designed carried out the surveys. Z.H.X. performed the geophysical data processing. W.X. and L.Z. prepared the manuscript with contributions from all co-authors.

Conflict of interest: Authors state no conflict of interest.

References

[1] Maithya J, Fujimitsu Y. Analysis and interpretation of magneto-telluric data in characterization of geothermal resource in Eburru geothermal field, Kenya. Geothermics. 2019;81(Sep):12–31.
[2] Wei H, Liu G, Gill J. Review of eruptive activity at Tianchi volcano, Changbaishan, Northeast China: implications for possible future eruptions. Bull Volcanol. 2013;75:1–14.
[3] Zhang ML, Guo ZF, Liu JQ, Liu GM, Zhang LH, Lei M, et al. The intraplate Changbaishan volcanic field (China/North Korea): a review on eruptive history, magma genesis, geodynamic significance, recent dynamics and potential hazards. Earth Sci Rev. 2018;187:19–52.
[4] Huang J, Zhao D. High-resolution mantle tomography of China and surrounding regions. J Geophys Res. 2006;111:B09305.
[5] Zhao D, Tian Y. Changbai intraplate volcanism and deep earthquakes in East Asia: a possible link? Geophys J Int. 2013;195:706–24.
[6] Harinarayana T, Zlotnicki J. Special issue of journal of applied geophysics "electrical and electromagnetic studies in geothermally active regions. J Appl Geophys. 2006;58(4):263–4.
[7] Guo Z, Wang K, Yang Y, Tang Y, John C. The origin and mantle dynamics of quaternary intraplate volcanism in Northeast China from joint inversion of surface wave and body wave. J Geophy Res Solid Earth. 2018;123:2410–25.
[8] Liu X, Xiang T. Cenozoic volcanoes and pyroclastic deposits in northeastern China: resources and hazards. Changchun: Jilin University Publishing House; 1997. p. 161 (in Chinese).
[9] Lustrino M, Wilson M. The circum-Mediterranean anorogenic Cenozoic Igneous province. Earth Sci Rev. 2007;81:1–65.
[10] Zhou JB, Wilde SA, Zhang XZ, Zhao GC, Zheng CQ, Wang YJ, et al. The onset of Pacific margin accretion in NE China: evidence from the Heilongjiang high-pressure metamorphic belt. Tectonophysics. 2009;478:230–46.
[11] Zhu G, Niu M, Xie C, Wang Y. Sinistral to normal faulting along the Tan-Lu fault zone: evidence for geodynamic switching of the east China continental margin. J Geol. 2010;118:277–93.
[12] Liu X, Zhao D, Li S, Wei W. Age of the subducting Pacific slab beneath East Asia and its geodynamic implications. Earth Planet Sci Lett. 2017;464:166–74.

[13] Qian C, Cui T, Jiang B, Li L, Chen H, Qin T. A study on the characteristics of late Cenozoic volcanic terrain in Changbaishan Mountain and its geological application. Quat Sci. 2014;34:312–24 (in Chinese with English abstract).
[14] Jin D, Cui T, Jin G. Observation and research on hot and warm springs in Changbaishan Tianchi volcano. Seismol Geol. 2003;25:121–7 (in Chinese with English abstract).
[15] Zhang M, Guo Z, Sano Y, Cheng Z, Zhang L. Stagnant subducted Pacific slab-derived CO_2 emissions: insights into magma degassing at Changbaishan volcano, NE. China. J Asian Earth Sci. 2015;106:49–63.
[16] Yan R, Woith H, Wang R, Wang G. Decadal radon cycles in a hot spring. Sci Rep. 2017;7:625. doi: 10.1038/s41598-017-12441-0.
[17] Xu ZH, Sun F, Xin W, Sun NR, Li FW, Niu JP. Formation and evolution of paleoproterozoic orogenic belt in southern Jilin, Jiao–Liao–Ji Belt, North China Craton: constraints from geophysics. Precambr Res. 2019;333:105433.
[18] Montanari D, Minissale A, Doveri M. Geothermal resources within carbonate reservoirs in western Sicily (Italy): a review. Earth Sci Rev. 2017;180–201.
[19] Yan BZ, Qiu SW, Xiao CL, Liang XJ. Relationship between the main faults and geothermal water anomaly in the Changbai Mountain basalt area. Hydrogeol Eng Geol. 2017;44:34–40 (in Chinese with English abstract).
[20] White DE, Williams DL. Assessment of geothermal resources of the United States – 1975. Office of scientific and technical information technical reports. US Department of the Interior, Geological Survey; 1975. p. 5–7.
[21] Muffler JLP. Assessment of geothermal resources of the United State. Reston, VA, USA: Geological Survey, Geological Div.; 1979. p. 12–26.
[22] Duan YH, Zhang XK, Yang ZX, Zhang CK, Zhao JR, Pan JS. Crystalline basement structure of Changbaishan Tianchi volcano area. Seismol Geol. 2003;25:501–8.
[23] Wang R, Zhang JQ, Guo EL, Zhao CL, Cao TH. Spatial and temporal variations of precipitation concentration and their relationships with large-scale atmospheric circulations across Northeast China. Atmosp Res. 2019;222:62–73.
[24] Zhang Y, Feng JY, He ZL. Classification of geothermal systems and their formation key factors. Earth Sci Front. 2017;24:190–8.